Proceedings of the 2006 IEEE/RSJ
International Conference on Intelligent Robots and Systems
October 9 - 15, 2006, Beijing, China

Characterization of Living Drosophila Embryos using Micro Robotic Manipulation System

Yantao Shen, U. C. Wejinya, Ning Xi, Craig A. Pomeroy, and Yonghui Xue
Department of Electrical and Computer Engineering
Michigan State University
East Lansing, Michigan 48824
Email: {shenya, wejinyau, xin, pomeroy3}@egr.msu.edu

Zhun Fan
Department of Mechanical Engineering
Technical University of Denmark
Lyngby, Denmark
Email: zf@mek.dtu.dk

***Abstract*— This paper aims at investigating and characterizing force behavior and mechanical properties of living Drosophila embryos using an *in situ* modeled PVDF (Polyvinylidene Fluoride) piezoelectric micro-force sensing tool with a resolution in the range of sub-μN. Drosophila embryo is one of the most studied organisms in biological research, medical research, genetics and developmental biology, and has implications in the cure of human diseases. In order to achieve high efficiency and accuracy during microinjection of genetic material into a Drosophila embryo, it is absolutely necessary to allow close monitoring of the magnitude and direction of microinjection forces acting on the embryo during injection. In this paper, a microrobotic biomanipulation platform integrating a two-axis (2-D) modeled PVDF micro-force sensor is used to implement force sensing during microinjection of living Drosophila embryos. Micro injection forces and membrane deformation of embryos in different stages of embryogenesis are found. Ultimately, the technology will provide a critical and major step towards the development of automated biomanipuation for batch microinjection of living embryos in genetics.**

I. INTRODUCTION

Genetic modification of Drosophila embryos has provided scientists biological means to finding the cause of diseases and development of medicine to cure these diseases. The fact that this type of research has human health care implications was confirmed by the award of the 1995 Nobel Prize in Physiology or Medicine to Edward B. Lewis, Christiane Nüsslein-Volhard, and Eric F. Wieschaus for their discoveries concerning the genetic control of early embryonic development. In their work, they have used the fruit fly, *Drosophila melanogaster*, as their experimental specimen. This organism is classical in genetics. The principles found in fruit fly, *Drosophila melanogaster*, applies to higher organisms including man [1].

The Drosophila genome can also provide critical information about human genes that are homologous in fruit fly [2]. To implement the research on Drosophila genome, one of the most important approaches and tasks is the injection of substances that affect the make-up of a cell or an organism. Micro injection such as transgenes, i.e. DNA structures that often consist of a gene and a control component, results in Drosophilas with new characteristics, since the transgene is integrated into the Drosophila's own DNA. This makes it possible to determine which genes are important for the development of the organism and which organs are affected [3]. However, most embryo injections are conducted manually. Operators often need very long training time to become proficient at the injection task.

The success rate of manual injection is disappointingly low, in the range of 2$\sim$4$\%$. The reason for this is that successful micro injection is greatly dependent on injection forces, injection speed, and trajectory [4]. To improve the quality of micro injection, a highly efficient micro injection system should be developed. Although existing micromanipulators can achieve extremely high accuracy in position, the success rate of micro injection is still at the low end due to the lack of an effective micro-force sensing and feedback mechanism.

Currently, there exist several developments on micro-force sensing used in characterizing micro injection of different cells or embryos. For instance, Sun et al. developed a microrobotic cell manipulation system, which employs a multiaxis capacitive force sensor with a tip diameter of 5μm to characterize the mechanical properties of Mouse Zona Pellucida [5]. In [6], the mechanical behavior of the Zebrafish embryo chorion is measured using an unmodeled PVDF force sensor with a 14.5μN resolution, an injection pipette of radius 14.6μm. The average penetration force of 737μN is also reported in [6]. In [7], a micrograting based force sensor integrated with a surface micromachined silicon-nitride probe for penetration and injection into Drosophila embryos is presented. An average penetration force of 52.5μN$\pm$13.2$\%$ with a 30μm diameter silicon tip was reported in their work.

In this paper, we developed an *in situ* PVDF (Polyvinylidene Fluoride) piezoelectric two-axis micro-force sensor with resolution in the range of sub-μN. In addition, a networked microrobotic biomanipulation platform integrating this developed two-axis (2-D) PVDF micro-force sensor is built. The tool is integrated with a glass pipette with an ultra sharp injecting tip of 1.685μm in diameter and 2.65° in angle. In addition, the dynamic model of the sensor is developed.

The developed micro-force sensor is integrated into a precision micro manipulator system and can easily be manufactured and assembled without using complex MEMS technology. Ultimately, the technology will provide a critical and major step towards the development of automated biomanipuation for batch injection of living embryos, which will facilitate the development of medicine for the cure of human diseases.

1-4244-0259-X/06/$20.00 ©2006 IEEE

II. MICRO-FORCE SENSING TOOL FOR MICRO INJECTION

A. Design and Modeling of 2-D Micro-Force Sensing Tool

For effective biomanipulation and micro injection, a self-decoupling two-axis (2-D) PVDF force sensing tool has been developed as shown in Fig. 1.

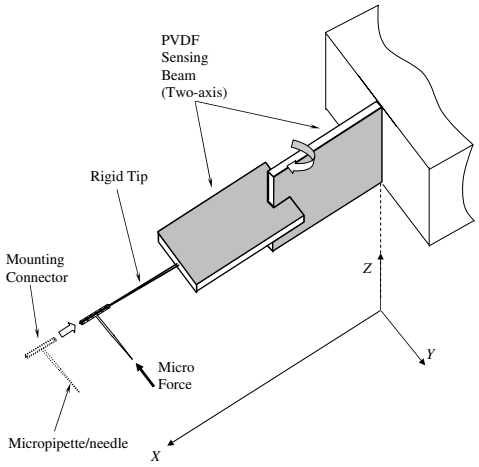

Fig. 1. Illustration of the 2-D PVDF micro-force sensing tool

The 2-D sensing tool is designed based on a serial connecting structure. In each direction, a PVDF composite beam is constructed. It can also be seen that this structure provides a decoupled force measurement in the Y and Z axis, which is due to the two PVDF composite beams' orthogonal configuration, as well as the strong shear forces along the Y and Z axis existing between the two PVDF beams. At the free end of the sensing tool, a rigid steel tip is attached, and a modified micropipette or needle is assembled to the end of the rigid tip. Following the configuration shown in Fig.1, for micro injection or operation in this paper, only 1-D (along Y axis) micro injection force is measured using the sensing tool.

Referring to the geometrical characteristic of the PVDF sensing layer, since the beam is much wider and longer than the thickness, the strain s_y along the width of the beam can be assumed to be zero [12]. Based on the piezoelectric transverse effect, the unit piezoelectric equation is: (without considering the pyroelectric effects due to use at stable temperature environment.) [8][16].

$$D_3(r,t) = d_{31}\sigma_s(r,t) \tag{1}$$

where $D_3(r,t)$ is the normal electric displacement of PVDF film. d_{31} is the transverse piezoelectric coefficient, $\sigma_s(r,t)$ denotes the unit stress of the PVDF sensing layer along the beam length, and $0 \le r \le L$.

The surface area polarization gives a charge $Q_s(t)$ across the PVDF sensing layer (surface area) S_A ($L \times W$):

$$\begin{aligned} Q_s(t) &= \int D_3(r,t)dS_A \\ &= \iint_{S_A} D_3(r,t)dydr. \end{aligned} \tag{2}$$

Using the mechanics of materials for a cantilever beam [14], the unit stress on the surface of the PVDF sensing layer can be obtained if the external load $f_c(t)$ acts along the micropipette

$$\sigma_s(r,t) = -cE_p\frac{\partial^2\omega_s(r,t)}{\partial r^2} \tag{3}$$

Since two-layer composite beam is considered (we omit the effect of very thin and low Young's modulus electrode layers at the top and bottom surfaces of PVDF layer.). c is the distance between the middle of the PVDF sensing layer and the neutral axis c_n of the composite beam. $\omega_s(r,t)$, the elastic deflection of the flexible composite beam caused by the micro force $f_c(t)$ along the micropipette. E_p is the Young's modulus of the PVDF sensing layer.

Since the bending charge is the same along the width of PVDF (s_y=0), we can write equation (2) as:

$$\begin{aligned} Q_s(t) &= \int_0^L d_{31}\sigma_s(r,t)Wdr \\ &= -cE_pd_{31}W\frac{\partial\omega_s(r,t)}{\partial r}|_0^L. \end{aligned} \tag{4}$$

A simplified and effective equivalent circuit model of a capacitor C_P can be used to represent the model of the PVDF sensing layer. And the output voltage $V_s(t)$ of the PVDF sensing layer caused by the micro force can be described by

$$V_s(t) = \frac{Q_s(t)}{C_P}. \tag{5}$$

By Laplace transformation, the electrical open-circuit transfer function of the sensing layer is given as:

$$V_s(s) = \frac{Q_s(s)}{C_P}. \tag{6}$$

To find the dynamic relationship between the sensing output V_s and the micro force f_c acting along the micropipette, we first describe a dynamic model of the flexible PVDF sensing beam based on the partial differential equation (PDE). Here the PDE describing the elastic deflection of the flexible composite PVDF sensing beam is a Bernoulli-Euler equation with additional terms due to the external force and moment at the free end of sensing beam as follows:

$$\begin{aligned} EI\frac{\partial^4\omega_s(r,t)}{\partial r^4} + \rho A\frac{\partial^2\omega_s(r,t)}{\partial t^2} &= f_c(t)\delta(r-L) \\ &+ f_c(t)L_0\frac{\partial(\delta(r-0)-\delta(r-L))}{\partial r} \end{aligned} \tag{7}$$

where E, I, L, L_0 and ρ represent the Young's modulus, inertia moment, length of beam, length of the rigid tip, and linear mass density of the composite beam respectively. We assume that $EI = E_bI_b + E_pI_p$, which is the flexural rigidity of the composite sensing beam, and $\rho A = \rho_bWh_b + \rho_pWh_p$ is the mass per unit length of the sensing beam. It is important to note that E_b, I_b represents the Young's modulus and inertia moment of the polyester layer, and I_p represents the inertia moment of the PVDF sensing layer. ρ_b, h_b represents the mass per unit density and the thickness of the polyester layer, and ρ_p, h_p

represents the mass per unit density and the thickness of the PVDF sensing layer. $\delta(\cdot)$ denotes the Dirac delta function.

By using the modal analysis method [9], and assuming that the deformation of the beam has infinite shape modes, the deflection $\omega_s(r,t)$ can be expressed as an infinite series in the following form :

$$\omega_s(r,t) = \sum_{i=1}^{\infty} \Phi_i(r) q_{si}(t) \tag{8}$$

where $\Phi_i(r)$ are the eigenfunctions satisfying the ordinary differential equation and $q_{si}(t)$ are the modal displacements caused by the micro force.

Using the Lagrange's equation of motion and orthogonality conditions [9], we have the differential equation corresponding to each shape mode of the composite beam of the sensing tool to be

$$\begin{aligned} EI\alpha_i^4 q_{si}(t) + \rho A \ddot{q}_{si}(t) = f_c(t)\Phi_i(L) \\ + f_c(t) L_0 [\Phi_i^{'}(L) - \Phi_i^{'}(0)] \end{aligned} \tag{9}$$

where a prime indicates the derivative with respect to position and a dot denotes the derivative with respect to time. α_i are the infinite set of eigenvalues. The natural frequencies ω_i of the composite sensing beam correspond to the α_i by

$$\omega_i = {\alpha_i}^2 \sqrt{\frac{EI}{\rho A}} \tag{10}$$

Then by the Laplace transformation of the above equation, the dynamic relationship between the modal displacements $q_{si}(s)$ and the external micro force is given as

$$q_{si}(s) = \frac{f_c(s)(\Phi_i(L) + L_0[\Phi_i^{'}(L) - \Phi_i^{'}(0)])}{\rho A(s^2 + \omega_i^2)}. \tag{11}$$

Based on equations (4) and (6), since $\omega_s(r,s) = \sum_{i=1}^{\infty} \Phi_i(r) q_{si}(s)$, by Laplace transform of equation (4), $Q_s(s)$ can be represented as

$$\begin{aligned} Q_s(s) &= -cE_p d_{31} W \omega_s^{'}(r,s) \mid_0^L \\ &= -cE_p d_{31} W \sum_{i=1}^{\infty} [\Phi_i^{'}(L) - \Phi_i^{'}(0)] q_{si}(s). \end{aligned} \tag{12}$$

Substituting equation (12) into equation (6), we have

$$V_s(s) = C_s \sum_{i=1}^{\infty} [\Phi_i^{'}(L) - \Phi_i^{'}(0)] q_{si}(s). \tag{13}$$

where $C_s = \frac{-cE_p d_{31} W}{C_P}$.

Subsequently, by combining equations (11) and (13), we have the dynamic sensing model, which denotes the dynamic relationship between the output voltage V_s of the PVDF sensing layer and the external micro force f_c along the Y axis (micro pipette) as follows:

$$\begin{aligned} \frac{V_s(s)}{f_c(s)} = C_s \sum_{i=1}^{\infty} \{ \frac{[\Phi_i^{'}(L) - \Phi_i^{'}(0)]\Phi_i(L)}{\rho A(s^2 + \omega_i^2)} \\ + \frac{L_0[\Phi_i^{'}(L) - \Phi_i^{'}(0)]^2}{\rho A(s^2 + \omega_i^2)} \}. \end{aligned} \tag{14}$$

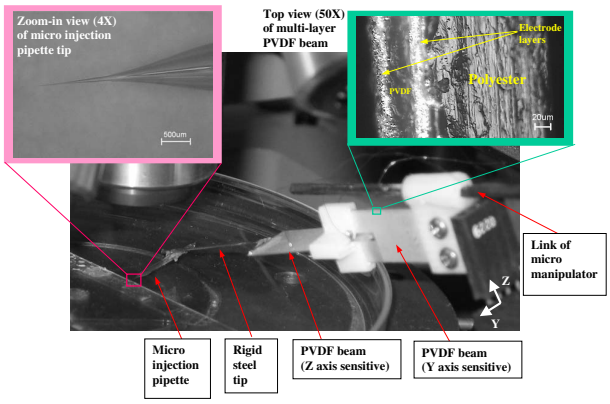

Fig. 2. PVDF sensing tool for micro injection.

To achieve the sensing voltage V_s, the PVDF sensing layer is interfaced with the PCI-DAS4020/12 analog/digital input/output board (Measurement & Computing Co.) in the PC through a developed instrumental amplifier circuit. The circuit was constructed using the AD549 ultralow input bias current operational amplifier (Analog Devices Co.) with a high input impedance $R_{in} = 10^{13}\Omega$ and low bias current $150fA$. Notice that $R_3 = R_4$ and $R_1 = R_2$. The amplifier circuit is used to buffer the open circuit voltage V_s of the PVDF sensing layer, and can convert the high impedance signal generated by the PVDF sensing layer to a low impedance voltage suitable for convenient coupling to the PCI-DAS4020/12 acquisition board. The circuit output V_{so} is an amplified and filtered approximation of the voltage V_s and can be sampled by the PCI-DAS4020/12 board. The maximum sampling frequency of PCI-DAS4020/12 is 20MHz with 12-bit A/D resolution. The loop time of the force sensing and acquisition is about 60μs. The transfer function between V_{so} and V_s can be represented as:

$$\frac{V_{so}(s)}{V_s(s)} = \underbrace{\frac{R_3}{R_1} \frac{sR_{in}C_P}{1 + sR_{in}C_P}}_{C_b}. \tag{15}$$

To further remove the 60Hz noise from the data acquisition system, a zero phase notch filter is added in the data collection system.

Finally, by considering the whole sensing system, the global transfer function is found

$$\begin{aligned} \frac{V_{so}(s)}{f_c(s)} = C_b C_s \sum_{i=1}^{\infty} \{ \frac{[\Phi_i^{'}(L) - \Phi_i^{'}(0)]\Phi_i(L)}{\rho A(s^2 + \omega_i^2)} \\ + \frac{L_0[\Phi_i^{'}(L) - \Phi_i^{'}(0)]^2}{\rho A(s^2 + \omega_i^2)} \}. \end{aligned} \tag{16}$$

Based on this dynamic equation, we can obtain the micro force $f_c(t)$ by measuring the output voltage $V_{so}(t)$ from the sensing PVDF when the initial values $f_c(t_0)$ and $V_{so}(t_0)$ are known.

B. Calibration and Sensing Performance

In this paper, as shown in Fig. 2, the developed two-axis PVDF sensing tool for micro injection is demonstrated. In the

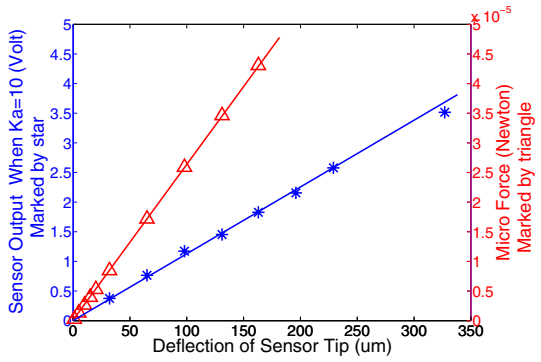

Fig. 3. Sensing output voltage vs deflection and micro force vs deflection.

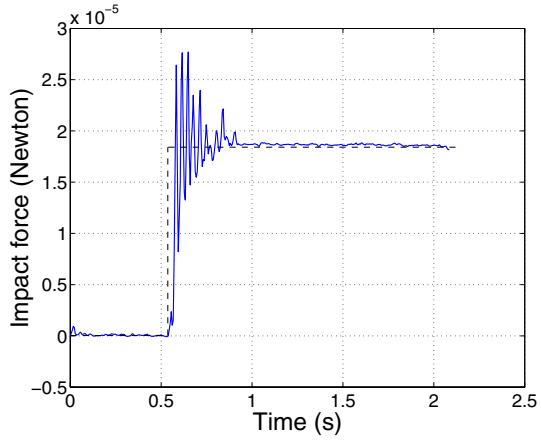

Fig. 4. Dynamic force sensing test: step impact and force hold.

sensing tool, a fine tipped micropipette with a tip diameter of 1.685 μm and a tip angle of 2.65° is attached to the end of the rigid steel tip. The micropipette is made by Omega Dot capillary tubing 30-30-1 of Frederick Haer & Co Inc. The Omega Dot capillary tubing is a unique product which revolutionized micropipette filling. This tubing is good for single cell recording and micro injection. Details can be found in [10].

The PVDF composite beam has four layers. Two thin layers are identical 6μm thick silver/urethane ink electrode layers with a low Young's modulus of $100MPa$. The other two layers are the 30 μm thick PVDF layer and 125 μm thick Polyester layer, respectively, with Young's moduli of $3 \times 10^9 Pa$ and $3.8 \times 10^9 Pa$. Since the Young's modulus of the PVDF or Polyester layer is 30 times more than the electrode layers, it is reasonable to neglect the effect of the electrode layers. The developed sensing tool has the following dimensions and related parameters: $L = 0.018348m$; $W = 0.010521m$; $L_0 = 0.05401m$; $C_P = 0.88 \times 10^{-9} F$; $d_{31} = 23 \times 10^{-12} C/N$; $c = 102.5 \times 10^{-6} m$; $h_p = 30 \times 10^{-6} m$; $h_b = 125 \times 10^{-6} m$; $E_p = 3 \times 10^9 N/m^2$; $E_b = 3.8 \times 10^9 N/m^2$; $\rho_p = 1.78 \times 10^3 Kg/m^3$; $\rho_b = 1.39 \times 10^3 Kg/m^3$; the amplified gain of the circuit is $K_a = \frac{R_3}{R_1}$=10.

Two sensing relationships were calibrated. That is, the relationship between the sensing output and the deflection of the sensing tip, and the relationship between the micro force and the deflection of the sensing tip.

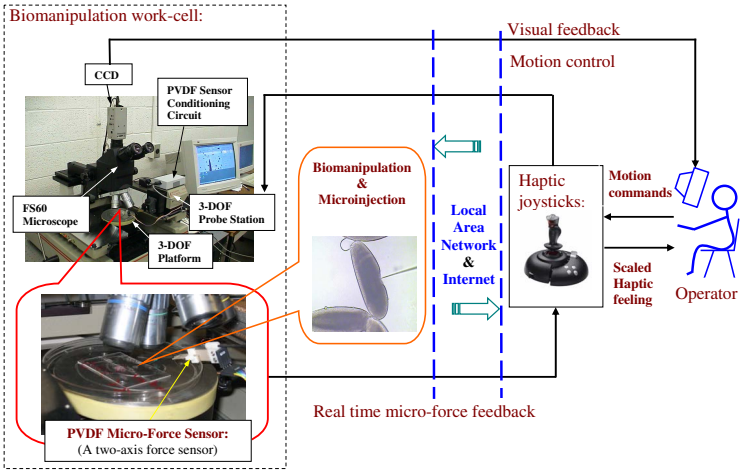

Fig. 5. Networked human/robot biomanipulation work-cell at MSU.

This calibrated force sensor has been successfully used in our previous work [11]. Both the sensing output-deflection and micro force-deflection curves are shown in Fig. 3. In this figure, the star marks (asterisks) represent the calibrated relationship between the sensing output and the deflection of the tip. The blue solid line through the asterisks is its simulation result based on the first shape mode equation derived from equations (8), (13), and (15). Similarly, the triangular marks denote the calibrated relationship between the micro force and the deflection of the tip. The red solid line through the triangular marks is the simulation result of the micro force vs deflection based on the first shape mode equation obtained from equations (8) and (11). Two calibration results verify the effectiveness of the developed sensing model. Fig. 4 shows the calibrated step force (the dash line) using the strain energy method [14][17], and the solid line shows an impact force obtained by the sensing tool using equation (16) in the first shape mode. By calibration, the sensitivity of the PVDF sensing tool was estimated to be 40.6mV/μN $\pm 6.5\%$, the resolution is in the range of sub-μN, which varies with the noise level and the amplified gain. The accuracy is $\pm 6.64\%$ in a full scale (the tip deflection within 250 μm). The spring constant k was estimated to be 0.264N/m $\pm 7.1\%$. The linearity was obtained as 6.63% in a full scale. All results show the performance of the developed force sensor.

III. NETWORKED HUMAN/ROBOT BIOMANIPULATION AND MICROINJECTION SYSTEM

Micro injection requires operations to be performed under a microscope. The visual information on the position of the micro injector and the workspace can be updated through real-time video feedback to the human operator as depicted in Fig. 5. By visually observing the injection operations, a human can plan and correct the next operation so as to achieve a

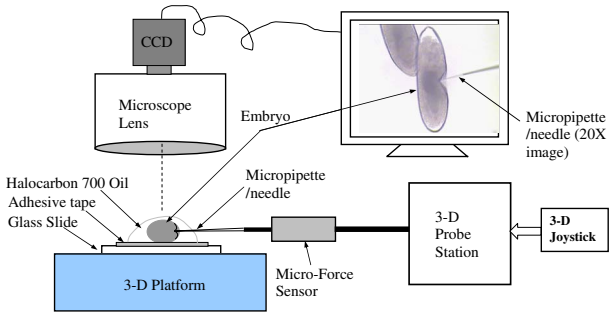

Fig. 6. Experimental configuration of micro injection of Drosophila embryos.

reliable and robust injection [13]. In this paper, we used both the micro-force and vision as essential action references for an integrated human/robot cooperative system. To ensure the synchronization of two data streams, an event-synchronization method proposed in [15] is employed. The developed network based biomanipulation work-cell is shown in Fig. 5. It consists of a 3-DOF micromanipulator (SIGNATONE Computer Aided Probe Station, a step resolution of 32nm.), a 3-DOF platform, a Mitutoyo FS60 optical microscope, a Sony SSC-DC50A CCD Color Video Camera, and a 3-DOF Microsoft SideWinder force feedback joystick. The 3-D platform can be controlled to convey the embryos or cells to the working area observed by the microscope. To reduce vibrations, an active vibration isolated table is used during biomanipulation/micro injection.

IV. FORCE MEASUREMENT AND MECHANICAL CHARACTERIZATION OF LIVING DROSOPHILA EMBRYOS

A. Micro Injection and Operation Configuration

In Fig.6, the microinjection/biomanipulation system configuration is shown. In this configuration, the embryos are held in place on the taped glass slide, which is placed on the 3-DOF platform as depicted in Fig. 5. The Y axis of force sensing tool is horizontally aligned to ensures that only a normal injection force is applied along the Y axis of the modeled PVDF force sensor. Since the prepared embryos are distributed on the taped glass slide with different orientations, the injection angle of Drosophila embryos will be different. In other words, the angle between the incidence direction of the pipette injector and the normal direction of the embryo membrane surface may be different. Based on this configuration, all force measurements and the characterization of mechanical properties of living embryos were implemented at a stable room temperature of $28°$C.

B. Force Profile of Micro Injection of Living Embryos

To measure the force of micro injection of embryo, the general operation procedures are as follows: first, the operator drives the joystick to move the micropipette tip along the Y axis to approach the embryo for injection. Once the tip penetrates the first membrane and goes inside of the embryo, in order to stop the pipette tip, the operator moves the micropipette tip back along the Y axis.

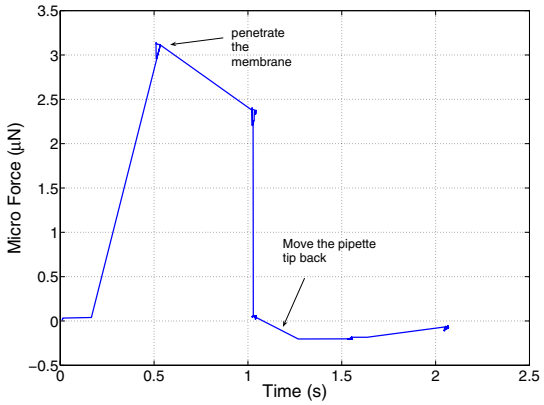

Fig. 7. Force profile of penetrating one membrane of fresh embryo.

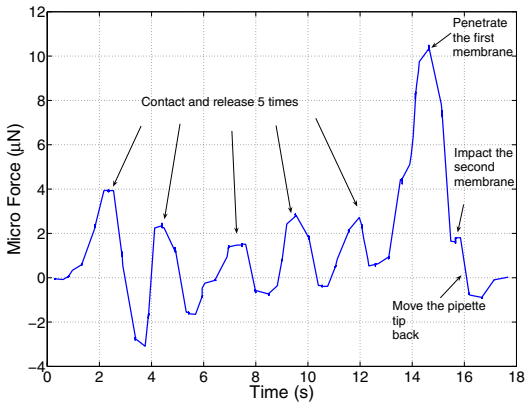

Fig. 8. Force profile of complex operation of living embryo

Fig. 7 shows the force profile measured by the developed PVDF sensing tool. In Fig. 7, the injection angle is $36.08°$, and injection speed is about 14.254μm/s. The puncturing force is approximately 3.1μN. Notice that, when the pipette tip is moved back, a negative force is shown due to fluid frictions and inertial effect. The embryo used is in stage 5 (Blastoderm Stage). All force measurements of living embryos were implemented in stable room temperature of $28°$C.

In addition, Fig. 8 shows the complex force profile including 5 contact-release operations and then the penetration of the embryo. Notice that, the speeds of the 5 contacts and 5 releases are diverse. Moreover, when the tip penetrates the first membrane into the embryo, the tip continues to impact the second membrane without puncturing it, then the tip is pulled out. These force behaviors are clearly demonstrated in Fig. 8. The embryo chosen is in Stage $11\sim12$ (Stage of Germ Band Elongation and Retraction). The injection angle is $43.1°$, and injection speed is about 44.4μm/s. The puncturing force is approximately 9.5μN. From the force profile, the penetration force and time of living embryo in Stage $11\sim12$ are greater and longer than the fresh embryo in Stage 5 demonstrated above. It is reasonable because the plasticity and density of the embryo

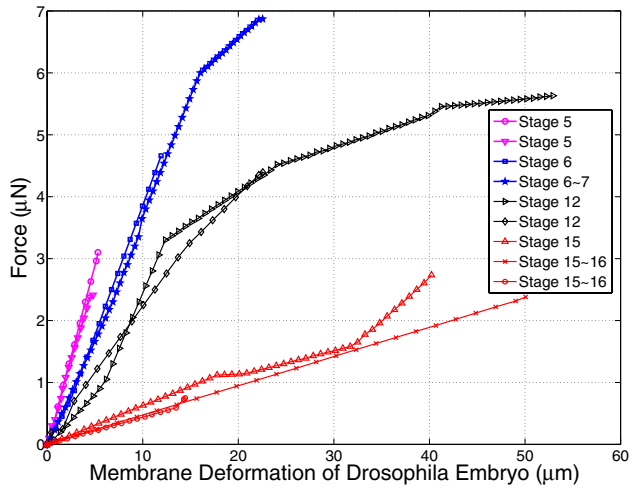

Fig. 9. Quantitative relationship between force and membrane deformation of living embryo in different stages.

membrane are both increased when the living embryo becomes gradually mature [18].

C. Quantitative Relationship Between Force and Membrane Deformation of Living Embryo in Different Stages

In this section, using the off-line membrane deformation measurement, which is based on the microscope images with a maximum resolution of 0.702μm/pixel, and the corresponding micro-force measurement, characterizing and quantifying the differences on mechanical properties of the living Drosophila embryos in different stages of embryogenesis is investigated. As a result, the quantitative relationship between the force and the membrane deformation is found and established. As shown in Fig. 9, several relationships on force-membrane deformation of diverse embryos in different stages are demonstrated. It can be seen that membranes of living embryo in the early stages have relatively smaller deformation with respect to the membranes of late stage embryos before being penetrated. In Fig. 9, from the early stages to the late stages, the stiffness of the embryo membrane reduces gradually. This implies that the plasticity of membrane of living Drosophila embryo gradually increase when the embryo becomes mature. In addition, the results in the same stage are repeatable by multiple experimentation. These quantitative results will improve the quality of micro injection for the study of the Drosophila genetic projects currently in existence.

V. Conclusion

In this paper, we investigated and characterized the force behavior and mechanical properties of living Drosophila embryos using an *in situ* PVDF (Polyvinylidene Fluoride) piezoelectric micro-force sensor. The model of the PVDF micro-force sensor was derived. Simulation and calibration results verify the effectiveness of the developed model. In addition, a networked microrobotic biomanipulation platform integrating the PVDF micro-force sensor in order to effectively measure micro injection forces of living Drosophila embryos was developed. Experimental results verifying micro injection force behaviors using an ultra sharp pipette tip were found. Ultimately, the technology will provide a critical and major step towards the development of automated biomanipuation for minimally invasive injection of living Drosophila embryos.

Acknowledgments

The authors would like to thank Mr. Martin S. Buckley and Miss. Li Li at the Arnosit's Lab of the Department of Biochemistry & Molecular Biology, Michigan State University for their great efforts on the preparation of fresh Drosophila embryos for this experiment. This research work is partially supported under NSF Grants IIS-9796300, IIS-9796287 and EIA-9911077, and ONR Grant N00014-04-1-0799.

References

[1] Press Release: The 1995 Nobel Prize in Physiology or Medicine. http://nobelprize.org/medicine/laureates/1995/press.html.

[2] G.M. Rubin, and E.B. Lewis, *A brief History of Drosophila's Contributions to Genome Research*, Science 287: 2216-2218, 2000.

[3] R. W. Bernstein and A. Dragland, *Microsurgery on Fruitfly Embryos*, In Features, GEMINI 2002/2003, Web Edition, http://www.ntnu.no/gemini/2002-06e/40-42.htm.

[4] Y. Kimura and R. Yamagimachi, *Intracyto-plasmic Sperm Injection in the Mouse*, Biology of Reproduction, vol. 52,no. 4, pp. 709-720, 1995.

[5] Y. Sun, K.-T. Wan, K. P. Roberts, J. C. Bischof, and B. J. Nelson, *Mechanical Property Characterization of Mouse Zona Pellucida*, IEEE Transactions on Nanobioscience, vol. 2,no. 4, pp. 279-286, 2003.

[6] D.-H. Kim, Y. Sun, S. Yun, B. Kim, C. N. Hwang, S. H. Lee, and B. J. Nelson, *Mechanical Property Characterization of the Zebrafish Embryo Chorion*, Proceedings of the 26th Annual International Conference of the IEEE EMBS, pp. 5061-5064, 2004.

[7] X. J. Zhang, S. Zappe, R. W. Bernstein, O. Sahin, C.-C. Chen, M. Fish, M. P. Scott, O. Solgaard, *Micromachined Silicon Force Sensor Based on Diffractive Optical Encoders for Characterization of Micro injection*, Sensors and Actuators A, vol. 114, pp. 197-203, 2004.

[8] *An American National Standard: IEEE Standard on Piezoelectricity*, ANS/IEEE Standard 176-1987, 1987.

[9] L. Meirovitch, *Elements of Vibration Analysis*, New York: McGraw-Hill, ch. 5, pp. 218, 1975.

[10] Data Sheet, *Capillary Tubing*, L022-D pp. 14-15, FHC Inc., website: www.fh-co.com/010300.

[11] Y. T. Shen, N. Xi, and Wen J. Li, *Force Guided Assembly of Micro Mirrors*, Proceedings of the IEEE/RSJ International Conference on Intelligent Robots and Systems, Vol. 3, pp. 2149-2154, 2003.

[12] M. S. Weinberg, *Working Equations for Piezoelectric Actuators and Sensors*, IEEE Journal of Microelectromechanical Systems, Vol. 8, no. 4, pp. 529-533, 1999.

[13] Y. Zhou, B. J. Nelson and B. Vikramaditya, *Fusing Force and Vision Feedback for Micromanpulation*, Proceedings of the IEEE International Conference on Robotics and Automation, pp. 1220-1225, 1998.

[14] W. H. Bowes, L. T. Russell, and G. T. Suter, *Mechanics of Engineering Materials*, John Wiley & Son, 1984.

[15] I. Elhajj, N. Xi, B. H. Song, M-M. Yu, W. T. Lo and Y. H. Liu, *Transparency and Synchronization in Supermedia Enhanced Internet-Based Teleoperation*, Proceedings of the IEEE International Conference on Robotics and Automation, pp. 2713-2718, 2002.

[16] *Piezo Film Sensors Technical Manual, Internet Version*, Measurement Specialties Inc., August, 1998.

[17] Y. T. Shen, N. Xi, U. Wejinya, and Wen J. Li, *High sensitivity 2-D force sensor for assembly of surface MEMS devices*, Proceedings of 2004 IEEE/RSJ International Conference on Intelligent Robots and Systems, Vol. 4, pp. 3363 - 3368, 2004.

[18] FlyMove, http://flymove.uni-muenster.de/Stages/StgTabelle.html.